ADVANCED OPTICAL MATERIALS
www.advopticalmat.de

Amplified Spontaneous Emission Realized by Cogrowing Large/Small Grains with Self-Passivating Defects and Aligning Transition Dipoles

Yujie Bai, Jiajun Qin, Lei Shi, Jia Zhang, Miaosheng Wang, Yiqiang Zhan, Han Zou, Stefan Haacke, Xiaoyuan Hou,* Jian Zi,* and Bin Hu**

This paper reports an amplified spontaneous emission (ASE) initiated by intrinsically passivating grain boundary defects and aligning transition dipoles in polycrystalline perovskite ($MAPbBr_3$) films. The method is developed by using concurrently occurring fast and slow growths to attach small grains on surfaces of large grains toward low-threshold ASE. This materials processing utilizes one-step solution method of mixing two $MAPbBr_3$ precursor ($PbBr_2$-based and $Pb(Ac)_2\cdot 3H_2O$-based) solutions to control two subsequent growths: quickly growing large grains followed by slowly growing small grains, leading to unique emitting centers from large grains and self-doping agents from small grains. With this design, spectral narrowing phenomenon is observed from the large grains with the full width at half maximum decreasing from 21 to 4 nm when the pumping fluence is increased from 2 to 10 μW, generating an efficient ASE. Concurrently, the observed ASE shows a linear polarization reaching 21.1%, indicating that the transition dipoles in large grains are linearly polarized with coherent interaction. Therefore, this processing strategy presents a unique method to intrinsically passivate grain boundary defects and align transition dipoles toward developing ASE by attaching small grains (serving as passivation agent) to the surfaces of large grains (functioning as light-emitting centers).

1. Introduction

Organic–inorganic hybrid perovskites with the structure of ABX_3 have demonstrated very interesting light-emitting properties with high photoluminescence (PL) quantum yield reaching 90% in solid state[1–3] as well as an amplified spontaneous emission (ASE) in the design ranging from 3D[4–8] to 2D[9–12] and nanostructures.[13–17] These interesting developments provide technical preparation to use solution-processing perovskites for developing thin-film lasing devices. ASE is an important phenomenon resulting from coherent light-emitting states in a gain medium toward developing lasing actions.[4,5,10,18] In general, an ASE can be realized by satisfying two conditions: i) polarizing the transition dipoles prior to the occurrence of radiative emission and ii) initiating the coherent interaction between transition dipoles. On the other hand, polycrystalline perovskite films are inevitably formed with grain boundary defects: the charged species (MA^+, I^-, and Br^-).[19–22] The grain boundary defects are detrimental to realizing ASE: quenching light-emitting states through nonradiative emission and preventing the coherent interaction between transition dipoles through Coulomb interaction.[23–27] Generally, the grain boundary defects can be largely decreased by extrinsically doping with different dopants (such as chloride or potassium) through solution processing methods.[28–32]

Here, we show that the grain boundary defects can be intrinsically passivated by subsequently growing large and

Dr. Y. Bai, Dr. J. Qin, Dr. L. Shi, Prof. X. Hou, Prof. J. Zi
State Key Laboratory of Surface Physics
Key Laboratory of Micro and Nano Photonic Structures (Ministry of Education) and Collaborative Innovation Center of Advanced Microstructures
Fudan University
Shanghai 200433, China
E-mail: xyhou@fudan.edu.cn; jzi@fudan.edu.cn
Dr. J. Zhang, Dr. M. Wang, Prof. B. Hu
Department of Materials Science and Engineering
University of Tennessee
Knoxville, TN 37996, USA
E-mail: bhu@utk.edu
Prof. Y. Zhan
Center for Micro Nano Systems
School of Information Science and Technology (SIST)
Fudan University
Shanghai 200433, China
E-mail: yqzhan@fudan.edu.cn
Dr. H. Zou, Prof. S. Haacke
Institut de Physique et Chimie des Matériaux de Strasbourg
Université de Strasbourg, CNRS
UMR 7504, 67000 Strasbourg, France
The ORCID identification number(s) for the author(s) of this article can be found under https://doi.org/10.1002/adom.201900345.

DOI: 10.1002/adom.201900345

small grains during spin-coating perovskite ($MAPbBr_3$) films, forming an essential configuration where wide-bandgap small grains at nanometers are attached to the surfaces of narrow-bandgap large grains at micrometers to form perovskite films through one-step solution method. Specifically, two ($MAPbBr_3$) precursor ($PbBr_2$-based and $Pb(Ac)_2\cdot 3H_2O$-based) solutions are mixed to realize concurrently occurring fast and slow growths to grow large grains at micrometers attached with small grains at nanometers. During spin-coating, the large and small grains are simultaneously grown with distinctly fast and slow growth rates based on composition selection. While the large grains are quickly grown through fast growth, the small grains are slowly grown on the surfaces of large grains to form perovskite ($MAPbBr_3$) films. Interestingly, with the concurrent fast and slow growths, the small grains can intrinsically passivate the boundary defects on the surfaces of large grains by neutralizing oppositely charged species during growth, leading to the self-passivation agents from small grains and the unique emitting centers from large grains. Furthermore, during concurrent fast and slow growths, the small grains can be anisotropically attached to the surfaces of large grains due to spatially constrained growth in thin films, leading to more and less small grains attached to the large grains in horizontal and vertical directions through film plane, respectively. Because the slow growth of forming small grains suppresses the fast growth of large grains, this leads to a possibility to create a certain orientation of large grains. Furthermore, when anisotropically distributed small grains neutralize the charge defects on the surfaces of large grains, this can cause a net polarization in large grains in vertical direction through film plane. This provides a precondition to realize linearly polarized transition dipoles. Therefore, subsequently growing large and small grains can lead to an efficient ASE by simultaneously passivating grain boundary defects and aligning transition dipoles in organic–inorganic hybrid perovskites.

2. Results and Discussion

Figure 1a shows the scanning electron microscopy (SEM) image of perovskite film prepared by mixing two ($MAPbBr_3$) precursor ($PbBr_2$-based and $Pb(Ac)_2\cdot 3H_2O$-based) solutions. It can be seen that the large grains formed with several micrometers are attached with small grains with about 100 nm. It should be noted that the $Pb(Ac)_2\cdot 3H_2O$-based precursor only leads to the growth of small grains due to slow crystallization rate (Figure 1b). By contrast, the $PbBr_2$-based precursor enables very fast crystallization to quickly grow isolates large grains as large as several micrometers during spin-coating prior to thermal annealing (Figure 1c). By mixing these two precursor solutions, subsequently growing large and small grains with micrometers and nanometers by mixing two precursor solutions forms unique configuration of attaching small grains on the surfaces of large grains to prepare perovskite ($MAPbBr_3$) films with mixed large/small grains through this simple one-step solution processing method. Here, the detailed crystallization processes occurring in our three perovskites can be shown with different colors in appearance indicated in Figure S1 (Supporting Information). The PL spectra were measured in transmission mode (Figure 1d) at different pumping fluences for three samples: mixed large/small grains, small-grains-only, and large-grains-only perovskite ($MAPbBr_3$) films. At the pumping fluence of 2 μW, the perovskite film with mixed large/small grains shows a broad spontaneous emission peaked at 535.7 nm with full width at half maximum (FWHM) of 22.8 nm. Interestingly, increasing the pumping intensity leads to a sharp peak at 546.3 nm appeared on the broad PL background, as indicated in Figure 1e. The FWHM reaches 4 nm when the pumping intensity is slightly increased to the threshold of 4.4 μW, presenting a spectral narrowing phenomenon in the perovskite film with mixed large/small grains. Simultaneously, the intensity of sharp peak is largely increasing above the threshold pumping intensity as shown in Figure 1f. Clearly, this spectral narrowing phenomenon represents an ASE enabled at the low threshold pumping intensity (4.4 μW, i.e., ≈60 μJ cm^{-2} per pulse) in the perovskite ($MAPbBr_3$) films prepared by attaching small grains to the surfaces of large grains to form mixed large/small grains. By contrast, the perovskites with large-grains-only and small-grains-only structures do not show any ASE, leaving the spectral width unchanged with the peaks at 540.7 and 531.7 nm, as the pumping intensity is continuously increased up to 80 μW (Figure 1e). By comparing with the PL spectra from large-grains-only and small-grains-only perovskite films, we can see that the ASE is essentially occurred in the large-grains component in perovskite film prepared with mixed large/small grains. Obviously, the large grains function as ASE centers in the mixed large/small grains where small grains are attached to the surfaces of large grains in the perovskite ($MAPbBr_3$) film. In general, an ASE can be realized when the light-emitting states develop a coherent interaction above the threshold pumping fluence in a gain medium. It has been observed that the I_2 and Br_2 based perovskites can demonstrate low threshold pumping fluences (1.6 and 68 μJ cm^{-2}).[33,34] We should note that the I_2 and Br_2 based perovskites have lower and higher exciton binding energies (13 vs 40 meV). The lower and higher exciton binding energies correspond to more and less spatially extended wavefunctions, leading to stronger and weaker interactions between excitons, respectively. As a consequence, the I_2 and Br_2 based perovskites can demonstrate lower and higher threshold pumping fluences to develop an ASE. Here, our perovskite ($MAPbBr_3$) films prepared with mixed large/small grains show an ASE at low threshold pumping intensity (4.4 μW, i.e., ≈60 μJ cm^{-2} per pulse). Although there are still many other strategies to realize low ASE thresholds in Br_2 based perovskites by some complicated methods such as nanostructure engineering[35] or low-temperature measurement,[36] we introduce a simple and new way to fabricate Br_2-based polycrystalline perovskite films with room-temperature ASE in this work.

It should be noted that ASE is a process which requires coherent emission to generate a spectral narrowing phenomenon while increasing pumping intensity.[4,37,38] The charged defects[39–42] at grain boundaries are seriously detrimental to the ASE due to nonradiative emission and screening effects of transition dipoles to prevent the coherent interaction between light-emitting states. Here, attaching the small grains to the surfaces of large grains presents an intrinsic method to decrease the defects on large grains, functioning as ASE centers, in the thin-film perovskites containing mixed large/small grains.

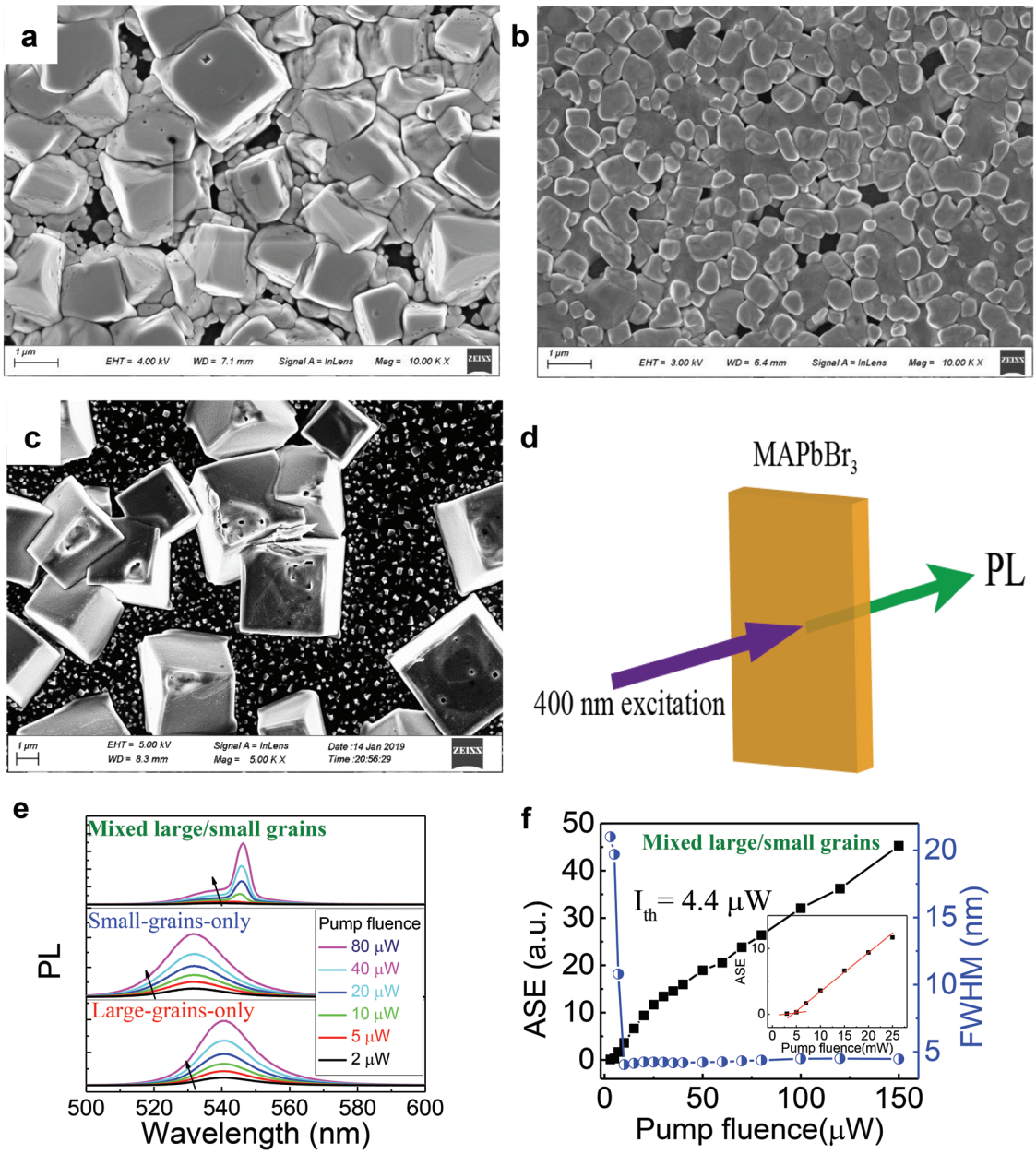

Figure 1. a) SEM results to show mixed large/small grains in perovskite ($MAPbBr_3$) film, with large grains around several micrometers and small grains around 100 nm. b) SEM results to show small-grains-only film. c) SEM results to show large-grains-only film. d) Schematic diagram of PL measurement. e) PL spectrum of different perovskite films under different pump fluences in transmission mode. Spectral narrowing phenomenon occurring in perovskite film prepared with mixed large/small grains. Broad PL in large-grains-only and small-grains-only perovskites at different pumping intensities, lacking spectral narrowing phenomenon. f) Linewidth (FWHM) and ASE intensity against pumping intensity.

The small and large grains have wider and narrower bandgaps (2.27 vs 2.22 eV) determined by optical absorption shown in Figure S2 (Supporting Information). The PL results in **Figure 2**a indicate that the thin-film perovskite ($MAPbBr_3$) with mixed large/small grains shows a broad PL spectrum (peaked at 535.7 nm) under low excitation intensity, which is located between large-grains-only (peaked at 540.7 nm) and small-grains-only (peaked ae 531.7 nm) films. We should note that potential wells formed at small/large grain interfaces due to the different bandgaps provide the precondition to confine the charged defects to mutually neutralize toward self-passivation of grain boundary defects, as illustrated in Figure S4 (Supporting Information). This is confirmed by PL lifetime results shown in Figure 2b. We can see that the perovskite ($MAPbBr_3$) film with mixed large/small grains demonstrates an enlarged PL lifetime of 7.92 ns relative to the large-grains-only (4.23 ns) and small-grains-only (4.01 ns) films in spontaneous emission at the pumping intensity (≈8 μJ cm^{-2} per pulse) much lower than threshold pumping fluence of realizing ASE. Interestingly, with the pumping fluence increasing toward ASE condition, the

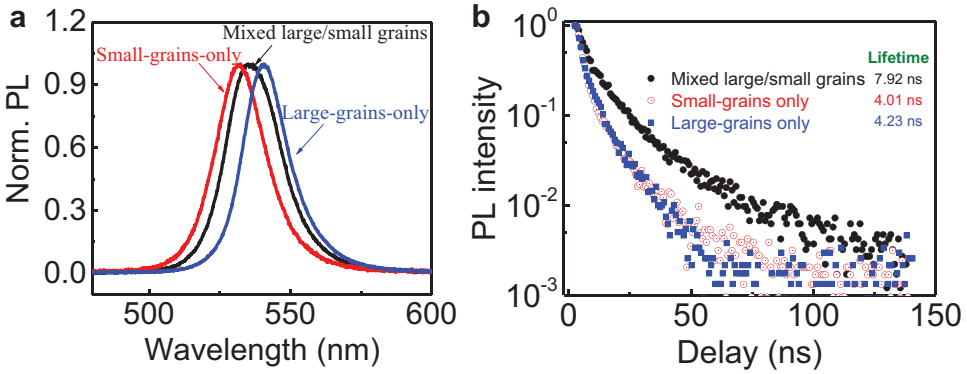

Figure 2. PL characteristics for three types of thin-film perovskites: with mixed large/small grains (black curve), small-grains-only (red curve), and large-grains-only (blue curve). a) PL spectra. b) PL lifetimes.

photoinduced transient absorption (TA) indicates that the large-grains component demonstrates a largely decreased lifetime (t_1 from 30.7 to 7.1 ps; t_2 from 160 to 44.9 ps) at 547 nm but the small-grains component shows only slightly changed (t_1 from 24.9 to 27.4 ps; t_2 from 185 to 198 ps) at 527 nm in the perovskite ($MAPbBr_3$) film with mixed large/small grains, as shown in **Figure 3**. Clearly, this lifetime study confirms that the large-grain component functions as ASE centers in the mixed large/small grains where small grains are attached to the surfaces of large grains to decrease the grain boundary defects.

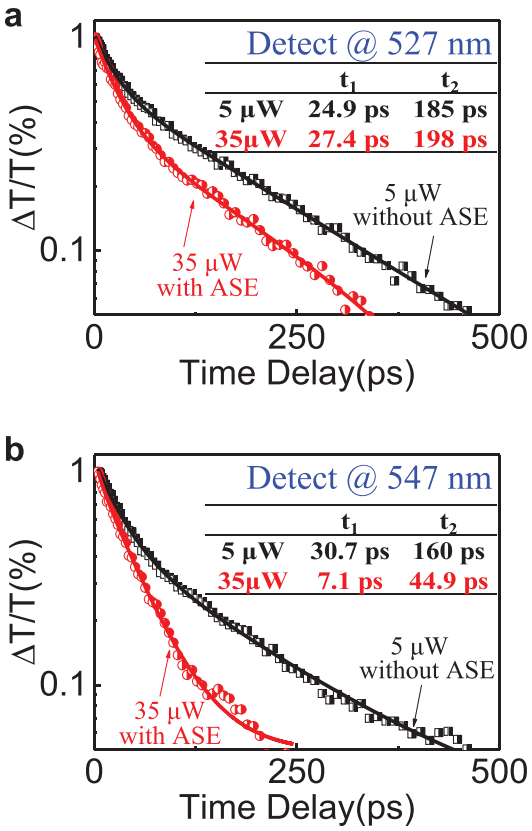

Figure 3. TA results at spontaneous emission (black curves with low pumping fluence of 5 μW) and ASE (red curves with pumping fluence of 35 μW) measured in transmission mode for perovskite film with mixed large/small grains. a) TA results detected at 527 nm corresponding to small-grain component. b) TA results detected at 547 nm corresponding to large-grain component.

To explore the polarization of transition dipoles accountable for ASE, the light emission was measured in transmission mode at variable angles ranging from 0° to 180° relative to the film plane (**Figure 4**a).[43–45] We can see in Figure 4b that the small-grains-only perovskite film shows the PL output with a circular spatial distribution between 0° and 180^0 where the maximum emission is occurred at 90^0 with the direction normal to film plane, while no emission is detected from the edge of the film (0° and 180°) at the pumping fluence up to 100 μW. Interestingly, the large-grains-only perovskite film gives rise to the PL output with an elliptical spatial distribution with dominant direction at around 80° at the pumping fluence of 100 μW, which provides an evidence to suggest that the transition dipoles are oriented with the direction normal to film plane. In the perovskite film with mixed large/small grains at the excitation intensity below threshold pumping fluence, the PL at 546 nm from large-grains-component shows a slightly elliptical spatial distribution with the dominant directions at 85° and 95° (Figure 4c). Here, we find that, at the excitation intensity (100 μW) above the threshold pumping fluence, the perovskite film with mixed large/small grains demonstrates an ASE with a more elliptical spatial distribution where the dominant directions occur at 140° and 40°, similar to the elliptical spatial distribution of transition dipoles in large-grains-only perovskite film. Furthermore, the broad emission detected at 527 nm from small-grains component gives a circular spatial distribution at the ASE condition, similar to small-grains-only perovskite film. Therefore, we can see that the transition dipoles accountable for ASE are from large-grains component in the perovskite film containing mixed large/small grains. Moreover, this observation indicates the following two points. First, large-grains and small-grains components are indeed coexisted in the perovskite film with mixed large/small grains but the ASE originates from large grains. Second, the existence of oriented dipoles with direction normal to film plane provides a precondition to realize an ASE. When the excitation intensity is below the threshold pumping fluence, the emission from lateral direction is largely decreased, resulting in the dominant emission at 90°. When the excitation intensity is above the threshold pumping fluence, the emission from lateral direction

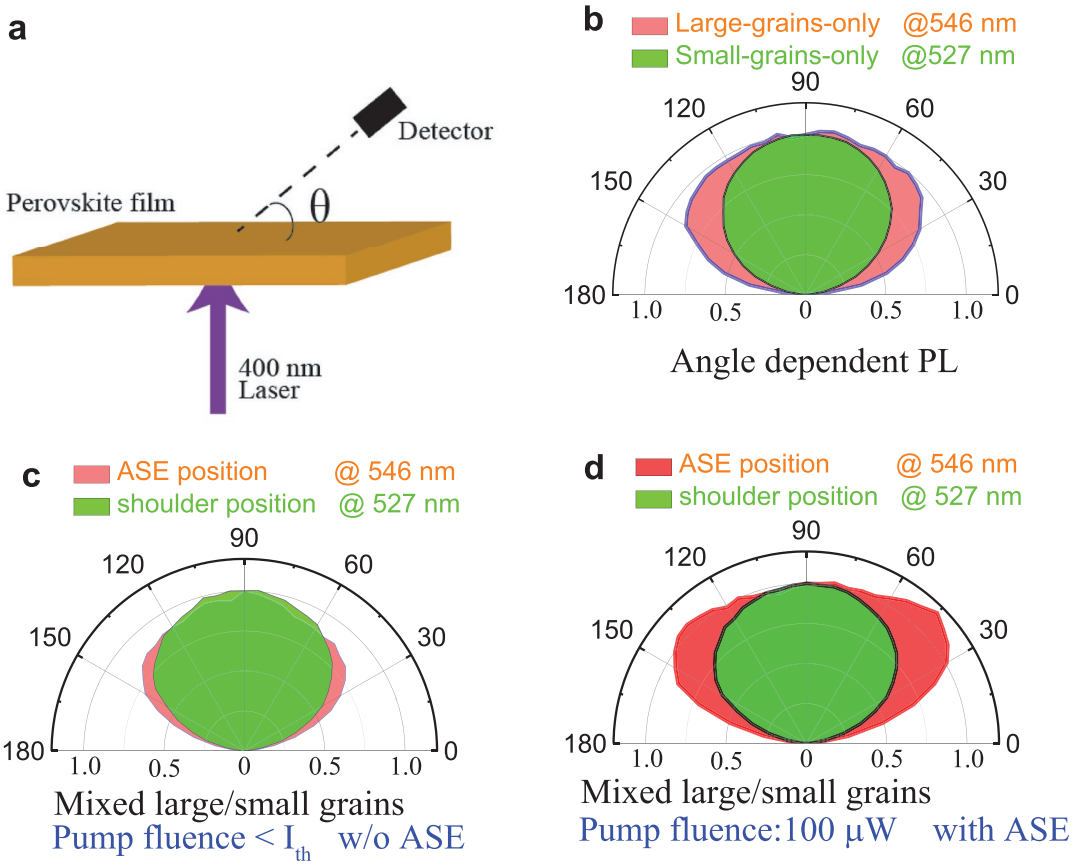

Figure 4. a) Schematic setup to measure angle-dependent PL intensity. The photoexcitation laser is perpendicular to the film plane. Angle-dependent PL intensity was measured by changing the detection angle in transmission mode. b) Angle-dependent PL intensity for large-grains-only and small-grains-only films, where spectral line-shapes do not change with pumping fluence. c) Angle-dependent PL intensity for perovskite film prepared with mixed large/small grains at low pumping fluence without ASE. d) Angle-dependent PL intensity for perovskite film prepared with mixed large/small grains at high pumping fluence with ASE.

is observed in the perovskite film with mixed large/small grains where the grain boundary defects are decreased by attaching small grains to the surfaces of large grains, which indicates that the light-emitting states are linearly polarized toward the normal direction to the film plane to generate an ASE.

In order to detect the possible ASE polarization in the direction normal to the film plane, we monitor light output intensity from the film edge by rotating a linear polarizer perpendicular to the film plane as shown in **Figure 5**a. This allows the detection of the polarization of light-emitting states in the direction normal to the film plane. Figure 5b shows that, when the ASE is realized, the light output from the film edge is largely changed by rotating the linear polarizer. The polarized emission detected from the edge is found in the perovskite film with mixed large/small grains. When the ASE occurs, the emission becomes linearly polarized with degree of polarization (DOP) of 21.1% with the polarized direction perpendicular to film plane. Clearly, when grain boundary defects are passivated by attaching small grains to the surfaces of large grains to form mixed large/small grains, the transition dipoles become orientated, providing a precondition to develop a coherent interaction toward ASE.

3. Conclusion

In summary, an efficient ASE is realized at low threshold intensity of 4.4 μW by using concurrent fast and slow growths to subsequently grow large and small grains with the configuration of attaching small grains on the surfaces of large grains to form perovskite ($MAPbBr_3$) films with mixed large/small grains. The PL lifetime studies show that attaching small grains to the surfaces of large grains can decrease the grain boundary defects, leading to the unique situation where the small grains function as self-passivation agents and the large grains act as emitting centers in the perovskite film. Furthermore, the angle-dependent light emission studies indicate that the transition dipoles are linearly oriented toward the normal direction to the perovskite film prepared by using concurrent fast and slow growths to form mixed large/small grains. Essentially, subsequently growing large and small grains results in anisotropic distribution of self-passivation agents of small grains around the large grains, providing the possibility of orientating transition dipoles in the emitting centers of large grains. Clearly, the oriented transition dipoles develop a coherent interaction and consequently generate an ASE above

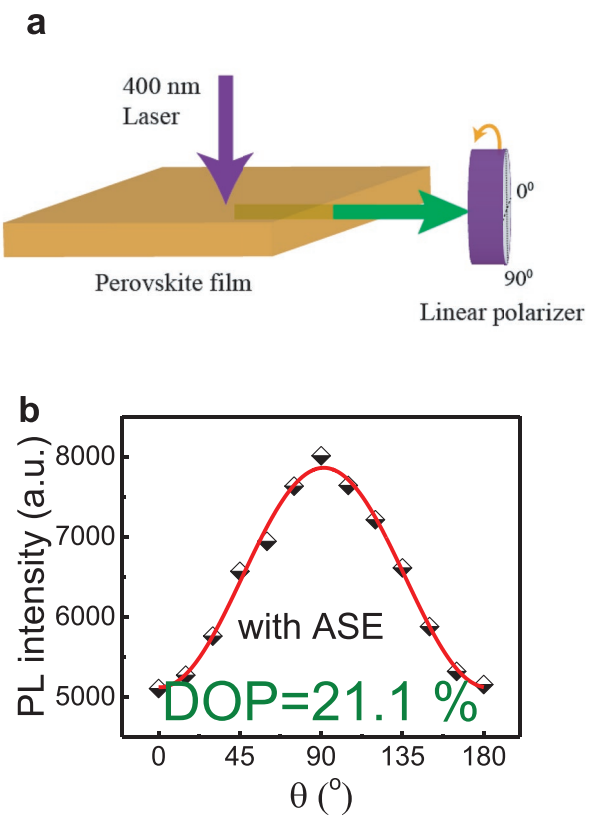

Figure 5. Evidence of coherent interaction between excited states in perovskite film mixing large/small grains. a) Schematic setup shown for the measurement on the polarization of ASE output. b) Output intensity shown as a function of detection angle (pumping fluence = 60 μW).

the low threshold pumping fluence of 4.4 μW. Therefore, using concurrent fast and slow growths to grow small grains on the surfaces of large grains through one-step solution processing method presents a unique strategy to simultaneously passivate grain boundary defects and orient transition dipoles to generate an ASE in perovskite ($MAPbBr_3$) films prepared with mixed small/large grains.

4. Experimental Section

Materials Preparation: All perovskite films were spin-casted onto glass/ITO/poly(3,4-ethylenedioxythiophene):poly(styrenesulfonate) (PEDOT:PSS) substrates. The PEDOT:PSS films with the thickness of 40 nm on ITO glass substrates were annealed at 150 °C for 0.5 h before spin-coating. The large-grains-only perovskite films were prepared by using *N*,*N*-dimethylformamide (DMF) solution with 1.58 mmol MABr and 1.5 mmol $PbBr_2$. The small-grains-only perovskite films were made by using DMF solution with 4.5 mmol MABr and 1 mmol $Pb(Ac)_2 \cdot 3H_2O$. Fast and slow growths for subsequently growing large and small grains were realized by mixing these two solutions together with volume ratio of 4:1 (more large-grains-only precursors). All three solutions are spin-cast at the rate of 3 krpm for 1 min, followed by thermal annealing at 60 °C for 30 min. Perovskite films were capsulated with polymethyl methacrylate (PMMA) for all measurements.

Formation Mechanism of Mixed Large/Small Grains: By using one-step solution method with $PbBr_2$ based precursor, the spin-coating leads to fast aggregation of $MAPbBr_3$ nanocrystals to enable the fast growth of isolated grains with several micrometers. In $Pb(Ac)_2 \cdot 3H_2O$ based precursor mixing MABr and $Pb(Ac)_2 \cdot 3H_2O$, the formation of MAAc and H_2O decreases the $MAPbBr_3$ crystallization rate, resulting in the small grains. By using the precursor where the two precursors are mixed together for spin-coating, the dominant $PbBr_2$ based portion can aggregate to form large grains and diffuse the $Pb(Ac)_2 \cdot 3H_2O$ based portion to the grain boundaries. After large grains are formed, the $Pb(Ac)_2 \cdot 3H_2O$ based source slowly grows on the boundaries of large grains, resulting in small grains. Therefore, the concurrently occurring fast and slow growths subsequently grow large and small grains with the configuration of attaching small grains on the surfaces of large grains to form polycrystalline perovskite ($MAPbBr_3$) films with mixed large/small grains. Particularly, slowly growing small grains on the fast-grown large grains can intrinsically neutralize the charged defects on the surfaces of large grains, leading to a self-passivation of grain boundary defects during entire growth. With this design, the large grains function as ASE centers while the small grains act as self-passivation agent. Furthermore, the concurrent fast and slow growths lead to anisotropic distribution of small grains around large grains while slowing growing the small grains under spatially constrained growth condition: horizontally favor growth and vertically unfavor growth through a film plane. This anisotropic distribution of small grains around large grains causes more and less neutralization of charged defects in horizontal and vertical directions, respectively. This provides a precondition to form a net polarization in vertical direction, presenting a possibility to polarize transition dipoles toward developing ASE. The surface morphology of perovskite film was characterized by scanning electron microscope (SEM, Zeiss sigma 300).

Optical Measurements: The pumping source was from a Coherent Legend regenerative amplifier (150 fs, 1 kHz, 800 nm) seeded by a Coherent Mira 900 oscillator (100 fs, 80 MHz). The 800 nm wavelength laser pulses were obtained by the regenerative amplifier, whereas the 400 nm wavelength laser pulses were generated by β-barium borate (β-BaB_2O_4, BBO) doubling crystal. The excited pulses of 400 nm were focused into point beam with the diameter of about 150 um. The ASE signals were collected by spectrometer (Horiba, iHR320)) and detected by a charge coupled device (Horiba, Synapse). The spatial dispersion of angle-dependent light intensity was characterized by angular resolved measurement setup (IdeaOptic, R1). The light emission at different angles was collected by fiber coupled spectrometer (IdeaOptic, PG2000 pro). The polarization of ASE output was characterized by combining a linear polarizer with the spectrometer.

For TA measurement, the same excitation source was used for measurements with a primary component sent to generate the pump pulses (400 nm, 150 fs, 1 kHz) and the secondary component further attenuated and focused into a 5 mm sapphire plate to generate the probe pulses. A short-pass filter (Thorlab FESF0750) was inserted into the probe beam to select probe window from 420 to 750 nm. The time delay between the pump and probe beams was regulated through a computer-controlled motorized translation stage in the probe beam. The temporal resolution between the pump and probe pulses was determined to be ≈150 fs (FWHM). The transmitted light was detected by a Si single point detector (Thorlab, DET36A2). The angle between the probe and pump beams was set at 30°. The intensity of the probe pulses transmitted through a monochromator (Horiba, iHR320) was measured by a lock-in-amplifier (Stanford Research Systems, SR830).

For PL lifetime measurement, the samples were excited by a 400 nm pulse laser (300 fs per pulse) from a home-built noncollinear optical parametric amplifier, seeded by the second harmonic of a Yb-doped fiber laser (TANGERINE, Amplitude System) with 50 kHz repetition rate and the average power of 10 μW. The beam size is 60 × 60 μm^2. The PL signals were collected by Streak camera (HAMAMATSU C10627).

Supporting Information

Supporting Information is available from the Wiley Online Library or from the author.

Acknowledgements

Y.B. and J.Q. contributed equally to this work. This work was supported by the Science and Technology Commission of Shanghai Municipality, the Ministry of Science and Technology of China (Grant No. 2012CB921400), and National Natural Science Foundation of China (NSFC) (Grant Nos. 11134002 and 11574049). B.H. also acknowledges the support from Air Force Office of Scientific Research (AFOSR) under the grant number FA 9550-15-1-0064, AOARD (FA2386-15-1-4104), and National Science Foundation (CBET-1438181).

Conflict of Interest

The authors declare no conflict of interest.

Keywords

amplified spontaneous emission, grain boundary engineering, passivation, perovskites, transition dipoles

Received: February 26, 2019
Revised: March 27, 2019
Published online:

[1] L. N. Quan, R. Quintero-Bermudez, O. Voznyy, G. Walters, A. Jain, J. Z. Fan, X. Zheng, Z. Yang, E. H. Sargent,. *Adv. Mater.* **2017**, *29*, 1605945.
[2] Z. Li, L. Kong, S. Huang, L. Li, *Angew. Chem., Int. Ed.* **2017**, *56*, 8134.
[3] S. A. Veldhuis, P. P. Boix, N. Yantara, M. Li, T. C. Sum, N. Mathews, S. G. Mhaisalkar, *Adv. Mater.* **2016**, *28*, 6804.
[4] G. Xing, N. Mathews, S. S. Lim, N. Yantara, X. Liu, D. Sabba, M. Gratzel, S. Mhaisalkar, T. C. Sum, *Nat. Mater.* **2014**, *13*, 476.
[5] Y. Jia, R. A. Kerner, A. J. Grede, B. P. Rand, N. C. Giebink, *Nat. Photonics* **2017**, *11*, 784.
[6] Y. Jia, R. A. Kerner, A. J. Grede, A. N. Brigeman, B. P. Rand, N. C. Giebink, *Nano Lett.* **2016**, *16*, 4624.
[7] R. Dhanker, A. N. Brigeman, A. V. Larsen, R. J. Stewart, J. B. Asbury, N. C. Giebink, *Appl. Phys. Lett.* **2014**, *105*, 151112.
[8] N. Arora, M. I. Dar, M. Hezam, W. Tress, G. Jacopin, T. Moehl, P. Gao, A. S. Aldwayyan, B. Deveaud, M. Grätzel, *Adv. Funct. Mater.* **2016**, *26*, 2846.
[9] M. Li, Q. Gao, P. liu, Q. Liao, H. Zhang, J. Yao, W. Hu, Y. Wu, H. Fu, *Adv. Funct. Mater.* **2018**, *28*, 1707006.
[10] M. Li, Q. Wei, S. K. Muduli, N. Yantara, Q. Xu, N. Mathews, S. G. Mhaisalkar, G. Xing, T. C. Sum, *Adv. Mater.* **2018**, *30*, 1707235.
[11] H. Zhang, Q. Liao, Y. Wu, Z. Zhang, Q. Gao, P. Liu, M. Li, J. Yao, H. Fu, *Adv. Mater.* **2018**, *30*, 1706186.
[12] F. O. Saouma, C. C. Stoumpos, J. Wong, M. G. Kanatzidis, J. I. Jang, *Nat. Commun.* **2017**, *8*, 742.
[13] K. Wang, G. Li, S. Wang, S. Liu, W. Sun, C. Huang, Y. Wang, Q. Song, S. Xiao, *Adv. Mater.* **2018**, *30*, 1801481.
[14] S. Yakunin, L. Protesescu, F. Krieg, M. I. Bodnarchuk, G. Nedelcu, M. Humer, G. De Luca, M. Fiebig, W. Heiss, M. V. Kovalenko, *Nat. Commun.* **2015**, *6*, 8056.
[15] T. J. S. Evans, A. Schlaus, Y. Fu, X. Zhong, T. L. Atallah, M. S. Spencer, L. E. Brus, S. Jin, X.-Y. Zhu, *Adv. Opt. Mater.* **2018**, *6*, 1700982.
[16] Y. Fu, H. Zhu, A. W. Schrader, D. Liang, Q. Ding, P. Joshi, L. Hwang, X. Y. Zhu, S. Jin, *Nano Lett.* **2016**, *16*, 1000.
[17] H. Zhu, Y. Fu, F. Meng, X. Wu, Z. Gong, Q. Ding, M. V. Gustafsson, M. T. Trinh, S. Jin, X. Y. Zhu, *Nat. Mater.* **2015**, *14*, 636.
[18] K. J. Kim, *Phys. Rev. Lett.* **1986**, *57*, 1871.
[19] M. Chen, X. Shan, T. Geske, J. Li, Z. Yu, *ACS Nano* **2017**, *11*, 6312.
[20] G. Nan, X. Zhang, A.-J. Mojtaba, A.-G. Zahra, S. D. Stranks, G. Lu, D. Beljonne, *Adv. Energy Mater.* **2018**, *8*, 1702754.
[21] J. F. Galisteo-Lopez, Y. Li, H. Miguez, *J. Phys. Chem. Lett.* **2016**, *7*, 5227.
[22] E. T. Hoke, D. J. Slotcavage, E. R. Dohner, A. R. Bowring, H. I. Karunadasa, M. D. McGehee, *Chem. Sci.* **2015**, *6*, 613.
[23] J. M. Frost, K. T. Butler, F. Brivio, C. H. Hendon, M. van Schilfgaarde, A. Walsh, *Nano Lett.* **2014**, *14*, 2584.
[24] Z. Fan, J. Xiao, K. Sun, L. Chen, Y. Hu, J. Ouyang, K. P. Ong, K. Zeng, J. Wang, *J. Phys. Chem. Lett.* **2015**, *6*, 1155.
[25] A. Stroppa, C. Quarti, F. De Angelis, S. Picozzi, *J. Phys. Chem. Lett.* **2015**, *6*, 2223.
[26] S. Liu, F. Zheng, N. Z. Koocher, H. Takenaka, F. Wang, A. M. Rappe, *J. Phys. Chem. Lett.* **2015**, *6*, 693.
[27] H. Röhm, T. Leonhard, M. J. Hoffmann, A. Colsmann, *Energy Environ. Sci.* **2017**, *10*, 950.
[28] S. Colella, E. Mosconi, P. Fedeli, A. Listorti, F. Gazza, F. Orlandi, P. Ferro, T. Besagni, A. Rizzo, G. Calestani, G. Gigli, F. D. Angelis, R. Mosca, *Chem. Mater.* **2013**, *25*, 4613.
[29] H. Lu, H. Zhang, S. Yuan, J. Wang, Y. Zhan, L. Zheng, *Phys. Chem. Chem. Phys.* **2017**, *19*, 4516.
[30] T. Wu, L. Collins, J. Zhang, P. Y. Lin, M. Ahmadi, S. Jesse, B. Hu, *ACS Nano* **2017**, *11*, 11542.
[31] M. Abdi-Jalebi, Z. Andaji-Garmaroudi, S. Cacovich, C. Stavrakas, B. Philippe, J. M. Richter, M. Alsari, E. P. Booker, E. M. Hutter, A. J. Pearson, S. Lilliu, T. J. Savenije, H. Rensmo, G. Divitini, C. Ducati, R. H. Friend, S. D. Stranks, *Nature* **2018**, *555*, 497.
[32] J. K. Nam, S. U. Chai, W. Cha, Y. J. Choi, W. Kim, M. S. Jung, J. Kwon, D. Kim, J. H. Park, *Nano Lett.* **2017**, *17*, 2028.
[33] F. Yuan, Z. Wu, H. Dong, J. Xi, K. Xi, G. Divitini, B. Jiao, X. Hou, S. Wang, Q. Gong, *J. Phys. Chem. C* **2017**, *121*, 15318.
[34] S. Ghimire, L. Chouhan, Y. Takano, K. Takahashi, T. Nakamura, K.-i. Yuyama, V. Biju, *ACS Energy Lett.* **2019**, *4*, 133.
[35] S. Lee, J. Park, B. R. Lee, E. D. Jung, J. C. Yu, D. D. Nuzzo, R. H. Friend, M. H. Song, *J. Phys. Chem. Lett.* **2017**, *8*, 1784.
[36] V. Sarritzu, M. Cadelano, N. Sestu, D. Marongiu, R. Piras, X. Chang, F. Quochi, M. Saba, A. Mura, G. Bongiovanni, *Phys. Status Solidi C* **2016**, *13*, 1028.
[37] G. S. Agarwal, *Phys. Rev. Lett.* **1986**, *57*, 827.
[38] S. Kéna-Cohen, S. R. Forrest, *Nat. Photonics* **2010**, *4*, 371.
[39] J. M. Azpiroz, E. Mosconi, J. Bisquert, F. D. Angelis, *Energy Environ. Sci.* **2015**, *8*, 2118.
[40] C. Eames, J. M. Frost, P. R. Barnes, B. C. O'Regan, A. Walsh, M. S. Islam, *Nat. Commun.* **2015**, *6*, 7497.
[41] H. Yu, H. Lu, F. Xie, S. Zhou, N. Zhao, *Adv. Funct. Mater.* **2016**, *26*, 1411.
[42] C. Zhao, B. Chen, X. Qiao, L. Ruan, K. Lu, B. Hu, *Adv. Energy Mater.* **2015**, *5*, 1500279.
[43] D. C. Marra, E. S. Aydil, S.-J. Joo, E. Yoon, V. I. Srdanov, *Appl. Phys. Lett.* **2000**, *77*, 3346.
[44] S.-Y. Kim, W.-I. Jeong, C. Mayr, Y.-S. Park, K. H. Kim, J.-H. Lee, C.-K. Moon, W. Brütting, J.-J. Kim, *Adv. Funct. Mater.* **2013**, *23*, 3896.
[45] R. Houdre, C. Weisbuch, R. P. Stanley, U. Oesterle, P. Pellandini, M. Ilegems, *Phys. Rev. Lett.* **1994**, *73*, 2043.

